Fuel Processing Technology 111 (2013) 1–13

Contents lists available at SciVerse ScienceDirect

Fuel Processing Technology

journal homepage: www.elsevier.com/locate/fuproc

Gasification of lignite in a dual fluidized bed gasifier — Influence of bed material particle size and the amount of steam

Stefan Kern *, Christoph Pfeifer, Hermann Hofbauer

Vienna University of Technology, Institute of Chemical Engineering, Getreidemarkt 9/166, 1060 Vienna, Austria

ARTICLE INFO

Article history:
Received 11 October 2012
Received in revised form 4 January 2013
Accepted 14 January 2013
Available online 17 February 2013

Keywords:
Gasification
Lignite
Dual fluidized bed
Olivine
Steam

ABSTRACT

The dual fluidized bed steam gasification system, developed by the Institute of Chemical Engineering at Vienna University of Technology, was originally developed for the utilization of woody biomass as feedstock, but during practical operation of the industrial sized plants of this system it turned out that fuel flexibility is the key issue for economic breakthrough. Therefore, gasification tests were carried out with lignite at different operating conditions at the dual fluidized bed pilot plant at Vienna University of Technology. Tests were performed with an input fuel power of 90 kW_{th}. Olivine was used as bed material and the applied particle size was 370 and 510 μm. The steam-to-carbon ratio was varied between 1.3 and 2.1 kg_{H2O}/kg_{carbon}. In addition to standard online measurements of the permanent gas components of the product gas, impurities like NH_3, H_2S and tar were also measured. It turned out that a lower amount of steam for fluidization caused a better performance of the gasification reactor in terms of product gas yield, carbon conversion and water conversion. The high catalytic activity of the lignite ash was also a reason for the high product gas quality producing low amounts of condensable hydrocarbons, like tar.

1. Introduction

Gasification of solid feedstock to a product gas for heat and power production or as a feedstock for synthesis processes attracts increasing interest since many years. Fluidized bed gasification turned out to be the most suitable reactor design for biomass gasification [1]. For coal gasification, the most common technology is entrained flow gasification with oxygen and steam as a gasification agent. Fluidized bed systems offer the benefit of a high fuel flexibility compared to entrained flow systems. Furthermore the supply of pure oxygen for entrained flow gasification is an expensive medium and, moreover, ecologically questionable. When inexpensive steam is used as a gasification agent, the product gas is free of nitrogen and the calorific value of the gas is high — values between 10 and 18 MJ/Nm^3_{db} can be reached [2,3]. The disadvantage for practical use of this gasification agent is that the gasification process becomes allothermal, so the heat for the endothermic gasification reactions has to be provided externally. A solution for the external introduction of the heat for gasification at an industrial scale can be provided by dual fluidized bed gasification (DFB).

The DFB technology separates the combustion reactor, which provides the energy for gasification, from the gasification reactor and pure steam is used as a gasification agent. Circulating bed material between these two reactors carries the heat from the combustion reactor to the gasification reactor. This gasification technology [4] has been successfully demonstrated at industrial scale, in Güssing [5] and Oberwart [6], Austria, on the 8 and 10 MW_{th} scale, respectively, since 2001 and 2008. Another plant in Villach, Austria with a fuel power of 15 MW_{th} is in operation since 2011 [7]. Further plants in Klagenfurt, Austria, Gothenburg, Sweden [8] and Senden, Germany, are currently under planning (Klagenfurt) construction (Gothenburg) or in the startup period (Senden), and will gain a fuel power of 15 MW_{th} (Senden), 25 MW_{th} (Klagenfurt) and 32 MW_{th} (Gothenburg). The Institute of Chemical Engineering at Vienna University of Technology operates a 100 kW DFB pilot plant for research purposes where research concerning different types of feedstock [9–12], operating conditions [13–15] and bed material properties [15,16] is carried out.

Especially at fluidized bed gasification conditions, fuels with a low content of volatile components, which means that gasification reactions dominate over the pyrolysis reactions, the reactivity of the char particles that have to react with the gasifying agent is a matter of interest for the design of the gasifier, as well as for the performance of the system. A higher reactivity of the coal or char results in higher system efficiency and, also, a lower gasification temperature can be chosen, which leads to higher cold gas efficiency [17]. Miura et al. [18] conducted investigations regarding factors that affect the reactivity of coal chars. The authors found that values like the surface area and pore structure of the fuel particles have an effect on the reactivity. On the contrary these simple char properties do not indicate that the reactivity is reliable. They classified coals into low-rank coals (C<80%) and higher-rank coals (C>80%) and stated that the reactivity of low-rank coals is mainly controlled by catalytic effects of minerals, such as calcium, potassium or sodium, whereas higher-rank coals' reactivity is affected mainly by the number of active sites in the coal matrix. The fact that there is no correlation between

* Corresponding author at: Tel.: +43 1 58801 166382; fax: +43 1 58801 16699.
E-mail address: stefan.kern@tuwien.ac.at (S. Kern).

0378-3820/$ – see front matter © 2013 Elsevier B.V. All rights reserved.
http://dx.doi.org/10.1016/j.fuproc.2013.01.014

properties of the fuels, like fixed carbon content, volatile matter or specific energy content, and the reactivity of coal was strengthened by Boyd and Benyon [19]. They also found an effect of inorganics on the reactivity.

Originally, the DFB system was used for the production of H_2-rich syngas out of woody biomass, but during commercial operation it turned out that fuel flexibility is a key issue for commercial breakthrough. To gain knowledge about the performance of a low-rank coal, lignite, from the Rhenish lignite mining region that is commercially used as a fuel for fluidized bed combustion at large scale, is used for the gasification tests discussed in this article. Other aspects that will be considered are the particle size of the bed material and the steam-to-carbon ratio. Therefore, tests with two different particle sizes and different fluidization conditions which mean different amounts of steam were performed.

2. Gasification of solid feedstock with steam

The main gasification reactions are shown in Table 1. These reactions are considered as equilibrium reactions with changing equilibrium conditions depending on gas concentrations, temperature and pressure. For the applied temperature range of fluidized bed gasification, equilibrium will normally not be reached. In the gasification reactor these reactions can take place at the same time and place and some reactions can be forced by operating parameters and by the utilization of catalytic active bed material. When applying steam for gasification, the water–gas shift reaction is forced, so carbon (C) is converted into H_2 and CO (Eq. (1)) and carbon which is also present in the gas in the form of CO can be converted to H_2 and CO_2 (Eq. (2)) already in the gasification reactor. This leads to a product gas with a high content of hydrogen. Based on the gasification reactions in Table 1, the overall reaction for gasification of solid hydro-carbon fuels can be expressed as Eq. (9) shows.

$$C_xH_y + x\cdot H_2O \rightarrow x\cdot CO + \left(x+\frac{y}{2}\right)\cdot H_2 \qquad \Delta H_{R,850} > 0 \tag{9}$$

Eq. (9) expresses that for each mole of carbon in the feedstock, 1 mol of water is required for a stoichiometrical conversion of the fuel. In the case of a common solid fuel for gasification, its main elements are not only carbon and hydrogen; oxygen can also make up a large part. For example, the oxygen content for wood pellets is 44 wt.%$_{daf}$ and for lignite 27 wt.%$_{daf}$. Including this aspect the overall steam gasification reaction results in Eq. (10).

$$C_xH_yO_z + (x-z)\cdot H_2O \rightarrow x\cdot CO + \left(x+\frac{y}{2}-z\right)\cdot H_2 \qquad \text{for} \qquad (x>z) \tag{10}$$

With Eq. (10), the amount of steam that has to at least be present during the process for a known composition of fuel can be defined. Using Eq. (11), we can see that this stoichiometric steam demand is

$$\phi_{H_2O} = (x-z). \tag{11}$$

For the tests in this publication, the feedstock can be expressed as the system $C_xH_yO_z$ free of sulfur and free of nitrogen. With the fuel analysis (see Table 4), the molarities of C, H and O results in $CH_{0.81}O_{0.34}$. With the knowledge of the fuel composition the stoichiometric steam demand can be calculated to:

$$\phi_{H_2O} = 41.06\,\mathrm{mol_{H_2O}/kg_{daf,N,S,Cl\ free}}$$

$$\phi_{H_2O} = 0.74\,\mathrm{kg_{H_2O}/kg_{daf,N,S,Cl\ free}}$$

In most of the cases of operating a gasifier, the real amount of H_2O in the system would differ from the amount stoichiometrically needed. To quantify the ratio of actual present H_2O and theoretically needed, an equivalent ratio for H_2O can be defined, similar to that which is used for combustion systems to determine the amount of air.

$$\lambda_{H_2O} = \frac{\dot{m}_{H_2O,actual}}{\dot{m}_{H_2O,stoich.}} \tag{12}$$

In real gasifiers, all the water introduced for conversion of the feedstock will not be converted due to several reasons. On the one hand, in order to maintain a good fluidization, a higher steam flow than stoichiometrically required is chosen. On the other hand, the aspects discussed before just consider the conversion of the feedstock to H_2 and CO. In a real case, a lot of simultaneous reactions take place such as pyrolysis, gasification, reforming and cracking as well as recombination reactions that lead to the final product gas composition.

By the facts mentioned above it can be assumed that the water–gas shift reaction takes place in the reactor especially in contact with catalytic active particles. In general, this reaction is desired, as a high hydrogen content is welcome in many cases. Moreover, materials that promote this reaction also force the decomposition of tar compounds [22] and reduce the required energy for the process due to its exothermic character. To quantify the distance to equilibrium, the model parameter is expressed as the logarithm of the ratio of the actual partial pressure product to the equilibrium constant (Eq. (13)). If $p\delta_{eq,CO\text{-}shift} < 0$, the actual state is still on the side of the reactants, so further reaction is thermodynamically possible. If $p\delta_{eq,CO\text{-}shift} = 0$, the water–gas shift equilibrium is fulfilled by the product gas composition and if $p\delta_{eq,CO\text{-}shift} > 0$, the actual state is on the side of the products. The latter case cannot be reached thermodynamically by the water–gas shift reaction; it is a result of the products generated by devolatilization and the other gasification reactions and the water content available in the product gas. If, for example, the gasifier is operated with a low amount of steam for gasification, the water content will be lower in the product gas. This moves the distance to water–gas shift equilibrium beyond 0 ($p\delta_{eq,CO\text{-}shift} > 0$). The water–gas shift reaction will then react towards its reactants and consume energy.

$$p\delta_{eq,CO-shift}(p_i,T) = \log_{10}\left[\frac{\Pi_i p_i^{v_i}}{K_{p,CO-shift}(T)}\right] \tag{13}$$

$K_{P,CO\text{-}shift}$ is the equilibrium constant of the water–gas shift reaction and can be determined via the database of HSC Chemistry [21]. For practical operation of gasifiers, there is another expression for the introduction of steam used. The steam-to-fuel ratio expresses the sum of water present in the system in relation to the total mass of introduced dry and ash-free fuel (Eq. (14)). As, initially, the steam is required for gasification of carbon particles (Eqs. (1) and (2)), the formulation of the so called steam-to-carbon ratio will also be used here (Eqs. (15) and (16)). This formulation makes comparisons for gasification of fuels with different origins easier, like coal and biomass, as coal with a higher heating value compared to wood, the required amount of fuel is lower to reach the same fuel power. This would result in very different steam-to-fuel ratios. Nevertheless for maintaining reproducible gasification conditions a constant steam-to-carbon ratio is essential.

$$\varphi_{SF,wt} = \frac{\dot{m}_{steam} + \nu_{H_2O}\cdot\dot{m}_{fuel}}{\left(1-\nu_{H_2O}-\nu_{ash}\right)\cdot\dot{m}_{fuel}} \tag{14}$$

Table 1
Equilibrium reactions for carbonaceous feedstock gasification [20,21].

Name of reaction	Chemical equation	$\Delta H_{R,850}$ [kJ/mol]	Equation
Water–gas (i)	$C + H_2O \leftrightarrow CO + H_2$	+135.7	(1)
Water–gas (ii)	$C + 2H_2O \leftrightarrow CO_2 + 2H_2$	+102.1	(2)
Boudouard	$C + CO_2 \leftrightarrow 2CO$	+169.4	(3)
Methanation	$C + 2H_2 \leftrightarrow CH_4$	−89.8	(4)
Oxidation (i)	$C + O_2 \leftrightarrow CO_2$	−394.9	(5)
Oxidation (ii)	$C + 0.5\ O_2 \leftrightarrow CO$	−112.7	(6)
Water–gas shift	$CO + H_2O \leftrightarrow CO_2 + H_2$	−33.6	(7)
Methane reforming	$CH_4 + H_2O \leftrightarrow CO + 3H_2$	+225.5	(8)

$$\varphi_{SC,wt} = \frac{\dot{m}_{steam} + \nu_{H_2O} \cdot \dot{m}_{fuel}}{\nu_C \cdot \dot{m}_{fuel}} \quad (15)$$

$$\varphi_{SC,mol} = \frac{\dot{m}_{steam} + \nu_{H_2O} \cdot \dot{m}_{fuel}}{\nu_C \cdot \dot{m}_{fuel}} \cdot \frac{12}{18} \quad (16)$$

For steam gasification the amount of the introduced water that is consumed for the gasification and steam reforming reactions is an indicator for the whole process. This value is called water conversion. The relative water conversion is defined as consumed amount of water per mass unit of converted fuel (Eq. (17)).

$$X_{H_2O,rel} = \frac{\dot{m}_{H_2O,con}}{\left(1 - \nu_{H_2O} - \nu_{ash}\right) \cdot \dot{m}_{fuel}} \quad (17)$$

The conversion of carbon in the gasifier to gaseous products can also be used as a key figure for the performance of the gasification process. This value is the carbon conversion. For a dual fluidized bed gasifier, one has to distinguish between the carbon conversion to product gas in the gasification reactor itself and the conversion of carbon of the whole system to product gas and flue gas. In the first case, the carbon conversion is the ratio of carbon leaving the gasification reactor in the form of gaseous products in the product gas stream to the introduced amount of carbon by the feedstock (Eq. (18)).

$$X_C = \frac{\dot{m}_{C_{PG}}}{\nu_C \cdot \dot{m}_{fuel}} \quad (18)$$

X_C can be used as a kind of parameter for determination of the amount of char that leaves the gasification reactor to the combustion reactor, neglecting char present in the product gas stream. For the whole system the carbon conversion is typically higher than 99%, as only entrained char to the gas streams occurs as carbon loss.

3. Materials and methods

3.1. The dual fluidized bed pilot plant at Vienna University of Technology

For the experiments in pilot scale, the 100 kW DFB pilot plant located at Vienna University of Technology was used [9]. The overall gasification reaction for steam gasification results in an endothermic effect (Eq. (9)), so energy in the form of heat is required to keep the gasification process running. The dual fluidized bed gasification system provides the heat for the gasification reactor by a separate combustion reactor while circulating bed material is carrying the heat from the combustion reactor to the gasification reactor. The basic principle of the dual fluidized bed gasification process is shown in Fig. 1 and a schematic drawing of the pilot rig is shown in Fig. 2. This system separates gasification and combustion, as two fluidized bed reactors connected together by loop seals are used. The fuel, usually biomass (here coal), enters the gasification reactor, a bubbling bed fluidized with steam, where drying, pyrolysis and heterogeneous char gasification take place at temperatures between 750 and 900 °C. The remaining residual char leaves the gasification reactor at the bottom together with the bed material, which circulates between the two reactors, through the lower loop seal to the combustion reactor. This reactor is implemented as a fast fluidized bed that is fluidized with air to maintain combustion of the residual char and additional fuel, if required. By burning char and additional fuel in the combustion reactor, the bed material is heated up, and after particle separation from the flue gas at the exit of the combustion reactor, it flows back to the gasification reactor via the upper loop seal. Both the lower and upper loop seals are fluidized with steam to ensure a high throughput of bed material and to avoid any leakage of gas between the reactors. In practical operations, the gasification temperature is normally controlled by the addition of fuel (e.g. recycled producer gas, part of the feedstock, etc., Fig. 1, broken lines) into the combustion reactor. In the case of the 100 kW pilot plant, light heating oil is used as fuel into the combustion chamber as it is easy to handle for processes on pilot scale. The pressure in both gasification and combustion reactors is close to atmospheric conditions. The main basic geometry data of the dual fluidized bed reactor system is summarized in Table 2. The process yields two separate gas streams at high temperatures: a high quality producer gas and a conventional flue gas. For the experiments discussed later in this article, the feedstock was fed directly into the bubbling bed via hopper 1 (Fig. 2).

3.2. Analytics

3.2.1. Measurement of main product gas composition

The composition of product gas is measured after the gasification reactor. The permanent gas components CH_4, H_2, CO, CO_2, and O_2 are measured by a Rosemount NGA 2000. The components N_2, C_2H_4 and C_2H_6 are measured using an online gas chromatograph (PerkinElmer Clarus 500). To avoid any contamination and damage of the gas analyzer and the column of the online gas chromatograph, the product gas is cleaned in terms of particulate matter and condensable components, as both gas measurement devices require dry gas. To maintain this, a

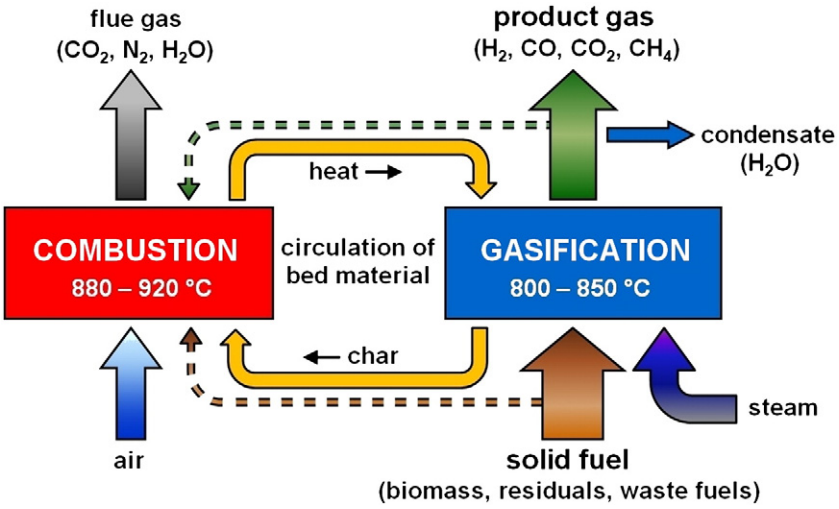

Fig. 1. Basic principle of the dual fluidized bed gasification process.

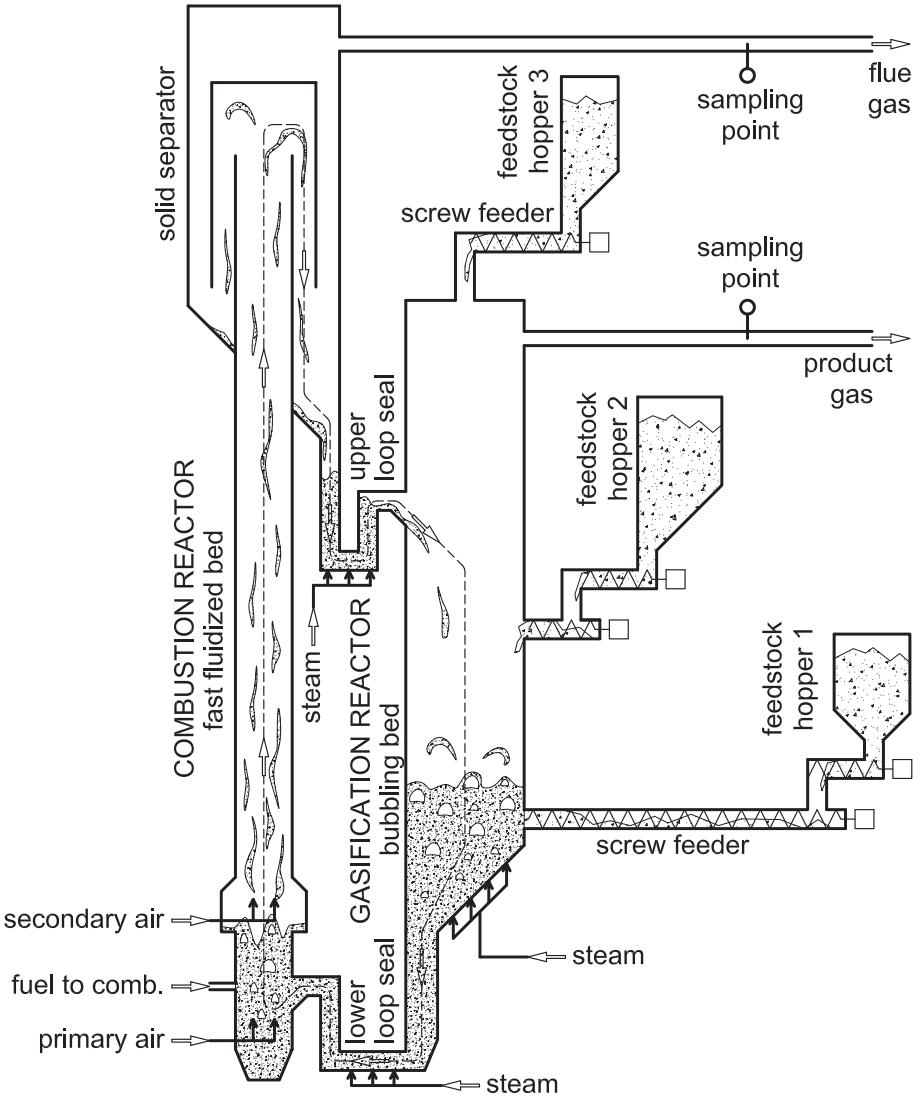

Fig. 2. Schematic of the dual fluidized bed gasification pilot plant at VUT.

gas cleaning line consisting of cooled impinger bottles filled with rapeseed oil methyl ester is used. The used gas cleaning line is explained in detail in a former work [23].

Table 2
Basic geometric data and main operation conditions of the dual fluidized bed system.

	Unit	Gasification reactor	Combustion reactor
Geometry	–	Conical bottom section with square-shaped upper freeboard section	Cylindrical
Reactor inner diameter	mm	304 (equivalent cylindrical diameter)	98
Reactor free height	M	2.35	3.9
Operable temperature range	°C	650–870	750–920
Fluidization agent	–	Steam	Air
Fluidization regime	–	Bubbling fluidized bed	Fast fluidized bed
Steam-to-fuel ratio	–	0.5–2.0	–
Bed material particle size (applicable)	Mm	200–800	

3.2.2. Tar measurement

Tar is sampled isokinetically with impinger bottles and, afterwards, gravimetric as well as GC–MS tars are determined. The tar sampling is applied discontinuously by condensing and dissolving the tars out of the product gas. The measurement method is based on the tar protocol according to CEN/TS 15439 [24] focusing on tars originating from biomass gasification. The applied method here differs in the used solvent, as CEN/TS 15439 proposes isopropanol (IPA), but here toluene is used. This allows a simultaneous detection of the water content in the product gas because water can be measured as a separate phase in the impinger bottles. Compared to IPA, using toluene as a solvent, the tar components benzene, toluene and xylene (BTX) cannot be detected. However, with toluene the separation performance for tar components larger than BTX is higher than for IPA. A schematic of the arrangement of the tar sampling line is shown in Fig. 3. The gas enters the heated sampling line, which consists of a cyclone and a glass wool-stuffed filled filter cartridge, where dust as well as condensed tar components is deposited. Afterwards, the gas is led through six impinger bottles, five of which are filled with toluene. The impinger bottles are located in a cooling bath cooled down to −8 °C by a cryostat. There the tars and steam condense. The liquid phases in the impinger bottles are unified and the aqueous phase is separated from the toluene phase. Afterwards, the amount of water is determined to calculate the water content in the gas stream. The amount of toluene is also marked down and a GC–MS sample is

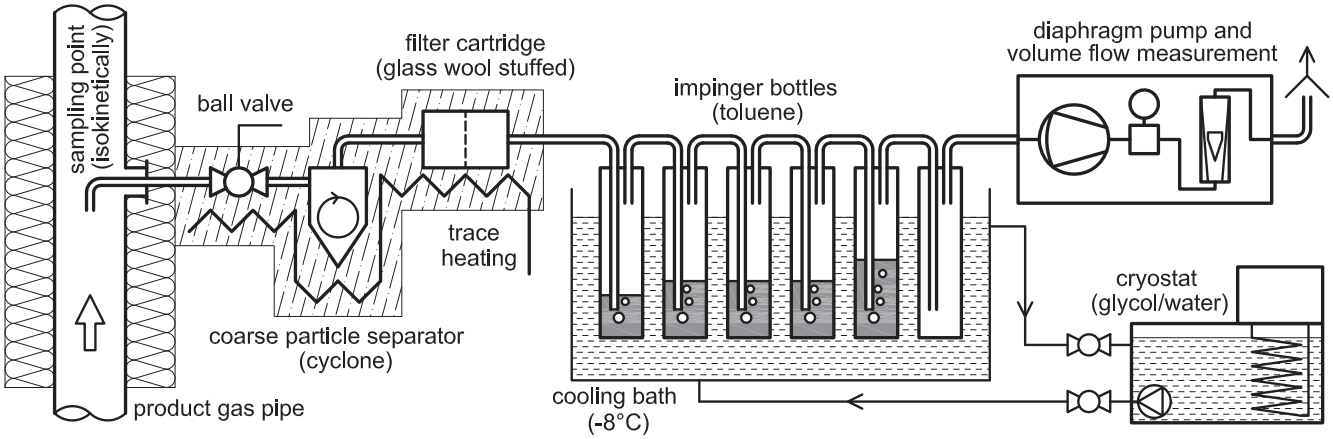

Fig. 3. Sampling line for tar, H_2O, entrained char and dust.

taken. Then the main part of the toluene is evaporated from the sample in a petri dish. To analyze the oil in the filter cartridge it is necessary to carry out a soxhlet extraction with IPA. Again a GC–MS sample of the IPA phase is taken. Afterwards the IPA phase is handled like the toluene phase. The results of the toluene phase and the IPA phase are added, which gives the amount of gravimetric tar in the product gas. The filter cartridge is reduced to its ashes by oxidizing the organic matter in a furnace. By weighing the cartridge before and after the muffle furnace treatment, the amount of entrained char and dust can be calculated. Finally, the GC–MS sample is analyzed in a GC–MS device to determine tar composition. This measurement method gains the following results:

- Gravimetric tar content
- GC–MS tar content
- GC–MS tar composition
- Water content
- Char load (organic matter)
- Dust load (inorganic matter).

3.2.3. NH_3 and H_2S measurement

For ammonia measurement, gas is sampled in a similar way to the tar measurements, using impinger bottles. The solvent used in this procedure is diluted sulfuric acid at a temperature of about −2 °C. The impinger bottles are placed in a glycol/ethanol mixture whose temperature is cooled down by a cryostatic temperature regulator. To avoid tar condensation in the pump, a bottle with toluene is added after the solvent for NH_3. After this procedure the concentration of ammonium ions in the sulfuric acid can be detected by a photometric method according to DIN 38 406 part 5 and ISO 7150.

Hydrogen sulfide is sampled using impinger bottles filled with an aqueous potassium hydroxide solution at a temperature of about −2 °C. Subsequently, the H_2S values were determined by potentiometry.

3.2.4. Flue gas measurement

The composition of the flue gas was measured after the combustion reactor with a Rosemount NGA 2000 (CO, CO_2, and O_2).

3.2.5. Fuel analysis

The feedstock for the gasification tests are analyzed by the "Testing Laboratory for Combustion Systems" at the Vienna University of Technology. The sampling and preparation of the fuels is done according to DIN 51701. After determination of the water content, described in DIN 51718 (drying at 30 °C to constant mass, grinding of the dried sample to a maximum particle size of 1 mm and drying of this sample at 106 ± 2 °C in an inert atmosphere to constant mass), the ash content is determined according to DIN 51719 by burning the sample to constant mass. C, H, N and S are measured by an elementary analyzer EA 1108 CHNS-O made by Carlo Erba. This is done by burning the sample under oxygen atmosphere. To make sure that CO formation is avoided, the gas passes a tungsten catalyst that ensures complete oxidation. Afterwards the gas passes a layer of copper at a temperature of 860 °C where free oxygen is bound. Here, nitrogen oxides are also reduced to N_2. As a result, the gas consists only of the components CO_2, H_2O, N_2 and SO_2 that can be detected. Present chlorine in the gas is absorbed in an aqueous perhydrol solution (H_2O_2), which is analyzed afterwards by capillary electrophoresis.

3.2.6. Analysis of inorganic components

Detection of the composition of the bed material and the inorganic matter of the fuels (ash) is done by X-ray fluorescence (XRF) analysis. This method uses the emission of characteristic fluorescent X-rays from a material that has been excited by bombarding with high-energy X-rays or gamma rays. The samples that have to be analyzed are melted at 1050 °C in a Merck Spectromelt and dumped at 400 °C on a stainless plate. The used XRF analyzer is a PANalytical Axios Advanced analyzer. The analysis is done under vacuum atmosphere with a rhodium anode, an excitation voltage of 50 kV and a tube current of 50 mA. As a result, the components are calculated as oxides.

3.3. Balance of the pilot plant

All of the online measured values during a gasification test are recorded by process-control software. With the gained data, mass and energy balances of the dual fluidized bed system can be calculated. For this purpose, the balance tool IPSEpro has been used. IPSEpro is a stationary, equation-oriented flow sheet simulation tool that has been developed for power systems [25].

3.4. Used bed material

The bed material that is used for the tests is olivine, provided by the Austrian manufacturer Magnolithe GmbH. During the last few years, olivine has become a widely known and used bed material and in-bed catalyst for fluidized bed gasification. It is a naturally occurring mineral that consists of silicate tetrahedra, which contains iron and magnesium $(Mg_{1-x}, Fe_X)SiO_2$. The content of iron and magnesium usually differs depending on the place of the olivine's mining. The effect of catalytic tar reduction by the use of olivine as bed material compared to silica sand in the DFB system was reported by Koppatz et al. [15]. By calcination of the olivine before using it, the catalytic activity can be improved essentially [26,27]. For long term utilization of olivine in biomass gasification systems, it was shown that the fuel ash interacts with the olivine particles and forms layers, rich in calcium, around the particles [28]. The effect on the gasification process is that the catalytic effect is improved a lot, so the tar values were found to be lower for the operation with

coated olivine particles compared to fresh uncoated olivine particles [22]. Also due to its high hardness and heat capacity, it is perfectly suitable for fluidized bed applications.

The bed material was used in two different mean particle sizes. The particle inventories are labeled as "coarse" particles (c), mean particle diameter $dp_{50,c} = 520$ μm and as "fine" particles (f), mean particle diameter $d_{p50,f} = 375$ μm. This particle sizes are classified as particle group B according to Geldart [29]. The graph of the size distribution of the fine bed material is printed in Fig. 4 and Fig. 5 shows the size distribution of the coarse olivine particles used for the tests. Based on the sieve analyses of the two different bed material sizes the mean Sauter diameters d_{sv} for both batches were calculated using the weighted mean diameter d_p of the analyses and the sphericity ϕ. The shape of the olivine particles was identified as approximately spherical, so the way to specify the mean Sauter diameter of the used bed material is $d_{sv} = \phi \cdot d_p$. With the sphericity $\phi = 0.9$ the mean Sauter diameter results to:

$d_{sv,f} = 370$ μm

$d_{sv,c} = 510$ μm

The results of the XRF analysis as well as the mechanical properties of the used olivine are listed in Table 3.

3.5. Feedstock

Lignite from the Rhenish lignite mining region (Germany) was used for the tests. The feedstock was provided with a particle size of 2–6 mm. This type of lignite is characterized by a relatively low content of sulfur, nitrogen and ash, compared to other types of lignite. The results of the proximate and ultimate analyses are summarized in Table 4.

4. Results and discussion

4.1. Overview

Gasification of lignite was carried out at three different operating points (OP1 –OP3). The general parameters of these tests are summarized in Table 5. In addition to investigating the general performance and the product gas composition of steam gasification of lignite, with this test series it was foreseen to study the influence of the bed material particle size and the amount of steam present in the gasifier on the performance of the system. For the gasification test OP1, the coarse bed material particles have been used. Up to now, this size of olivine particles was used for most of the tests as well as for all individual applications. However, most of the tests were done with biomass where the fuel mass flow has to be higher compared to coal or lignite due to the lower heating value of biomass. This leads to a higher steam-to-fuel ratio for lignite, as a certain amount of steam has to be introduced to maintain the bubbling fluidized bed. The idea was to use smaller particles to be able to lower the steam-to-fuel ratio to values that are well-established for steam gasification. This is reached with OP3, where a steam-to-fuel ratio of 0.9 kg_{H2O}/kg_{daf} was achieved. For the operation of OP2 the amount of steam was the same as for OP1 to investigate the influence of the bed material size at the same operating conditions. OP2 can be compared with OP3 for detecting the influence of the steam-to-carbon ratio (φ_{SC}) on the system. For each test, a new batch of 100 kg of olivine was used. Tar was sampled at every operating point whereas H_2S and NH_3 were only sampled at OP1, as their release to the product gas is relatively constant if the feedstock composition and the gasification temperature are constant.

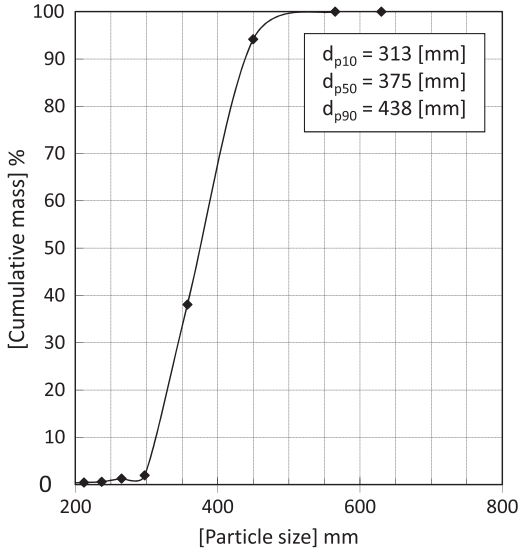

Fig. 4. Particle size distribution fine olivine particles.

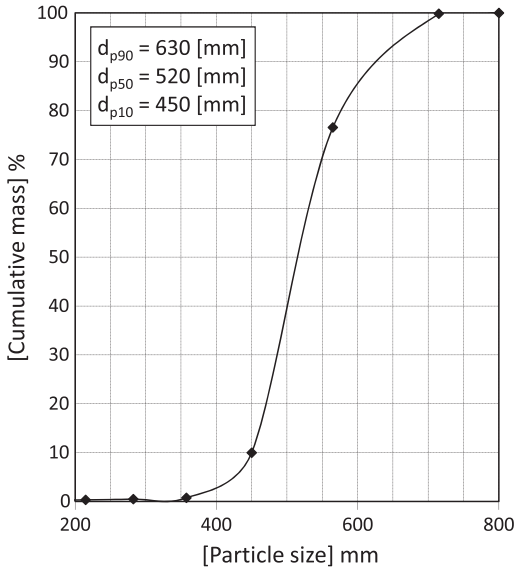

Fig. 5. Particle size distribution coarse olivine particles.

4.2. Key data, general gasification results

A first view into the behavior of the gasification of lignite in the dual fluidized bed system can be made by highlighting the fluidization conditions in the system and the temperature profiles in the gasifier at the

Table 3
Chemical composition and mechanical properties of the used olivine.

Composition	Unit	Olivine
Na_2O	wt.%	0.43
MgO	wt.%	46.76
Al_2O_3	wt.%	0.40
SiO_2	wt.%	39.84
P_2O_5	wt.%	0.03
SO_3	wt.%	0.06
K_2O	wt.%	0.32
CaO	wt.%	0.90
Cr_2O_3	wt.%	0.28
MnO	wt.%	0.15
Fe_2O_3	wt.%	10.32
NiO	wt.%	0.31
Cl	wt.%	0.10
Others	wt.%	0.11
Hardness	Mohs scale	6–7
Particle density	kg/m^3	2850

Table 4
Proximate and ultimate analyses of the feedstock (lignite).

Component	Unit	Dry basis	As used
Water content	wt.%	–	18.63
Ash content		4.23	3.44
C		65.53	53.32
H		3.75	3.05
N		0.84	0.68
O		25.22	39.16
S		0.38	0.31
Cl		0.05	0.04
Volatile matter		51.8	42.2
Fixed carbon	MJ/kg	48.2	39.22
LHV		24.31	19.33

different operating points. An overview about the fluidization regime is presented in Table 6. The velocities U_{mf}, U_t and their ratios with the actual superficial velocity in the gasification and combustion reactor can be used for characterization of the fluidized bed system. The values for the gasification and the combustion reactor are calculated for the mean Sauter diameter d_{sv}. In the gasification reactor, the bubbling fluidized bed is operated with a comparably low superficial velocity (U_g), but still between 2.7- and 6.0-times higher than U_{mf}. The fluidization regime in the combustion reactor has to be above the terminal velocity for a single particle (U_t).

The temperature profile in the gasification reactor is drawn in Fig. 6. This diagram illustrates that the temperature over the height of the reactor is changing due to several impacts on the system. The hot bed material, which transports the heat from the combustion reactor to the gasification reactor, is recirculated to the gasification reactor in the lower part of the freeboard. This causes a local hot spot where the highest temperature in the reactor is measured. A cold area is produced where the superheated steam for fluidization is introduced into the bubbling bed, because the steam temperature (approx. 300 °C) is significantly lower than the temperature of the bed material. Due to good intermixing of steam, bed material and fuel particles, and the high heat capacity of the bed material, the temperature decrease is limited. The set point for the gasification temperature (850 °C for OP1–OP3) is chosen at the height in the middle of the bubbling bed. In this area the fuel is also fed into the gasifier. In the middle and upper section of the freeboard, the temperature drops slightly in a constant way due to heat losses and energy-consuming reactions like steam reforming and cracking reactions as well as pyrolysis and gasification of entrained particles in the freeboard.

For OP1 and OP2 it can be seen that the temperature profiles are quite close to each other compared to OP3. OP3 shows the most distinctive temperature profile. At this operating point, the recirculated hot bed material has the highest temperature, but this energy is consumed in the reactor, as the lowest temperature is also measured in this third test run. This aspect is interesting, as, due to the lower amount of steam used in OP3, it was expected that less energy is utilized for heating up the steam in the reactor. An aspect that could explain this is that the endothermic gasification reactions are forced. This aspect will be discussed later when viewing the product gas yield. This could also be the reason why the bed material is heated up to a higher temperature in the combustion reactor, as the bed temperature in the gasification reactor was held to the set point of 850 °C.

Table 5
General parameters of the gasification tests.

Value	Unit	OP1	OP2	OP3
Particle size bed material	–	Coarse	Fine	Fine
Steam-to-carbon ratio, φ_{SC}	kg_{H2O}/kg_{carbon}	2.1	2.1	1.3
Steam-to-fuel ratio, φ_{SF}	$kg_{H2O}/kg_{fuel,daf}$	1.4	1.4	0.9
Fuel power lignite	kW		90	
Gasification temperature bubbling bed	°C		850 ± 2	
Mean temperature riser	°C	900	906	902
Fuel mass flow	kg/h	16.9	17.0	16.9
Fuel size	mm		2–6	
Initial bed material inventory	kg		100	
Batchwise sampling	–	Tar, NH_3, H_2S	Tar	Tar

4.3. Main product gas composition

The dual fluidized bed gasification process yields two separate gas streams, a product gas stream (gasification reactor) and a conventional flue gas steam (combustion reactor). The product gas primary consists of the gas components hydrogen (H_2), carbon monoxide (CO), carbon dioxide (CO_2), methane (CH_4), ethylene (C_2H_4), ethane (C_2H_6) and unconverted water (H_2O). The difference of the sum of these main components to 100% of gas components is made up by the following components or impurities:

- A nitrogen (N_2) content <1.5 $vol.\%_{db}$ can be present in the product gas as N_2 is used in the process as gas for inertization of the fuel feeding system.
- Gaseous C_2–C_5 hydrocarbons that are not detected with the applied measurement devices.
- Hydrogen sulfide (H_2S) in the product originating from the sulfur content in the fuel and
- Ammonia (NH_3) in the product originating from of the nitrogen in the fuel.

Fig. 7 provides the product gas composition for the three operating points. The H_2 content ranged between 48.2 and 50.7 $vol.\%_{db}$, CO between 25.3 and 29.5 $vol.\%_{db}$, CO_2 between 12.9 and 15.1 $vol.\%_{db}$ and the CH_4 content was in all cases very close to 4.4 $vol.\%_{db}$. These values for the gasification of lignite prove the significant influence of the feedstock of the system. Compared to the gasification of biomass the H_2 content is massively higher (about 40 $vol.\%_{db}$ in case of wood) and the CH_4 content considerably lower (about 11 $vol.\%_{db}$ in case of wood) [9,15]. C_2H_4 and, especially, C_2H_6 were present at a very low amount for biomass and coal gasification in general. C_2H_4 was found to be 0.8 ± 0.1 $vol.\%_{db}$ and C_2H_6 was 0.1 $vol.\%_{db}$ for all operating points. The lower heating value for the dry product gas was not affected, as it stayed constant around 11 MJ/Nm^3_{db}. The highest H_2 content was reached during OP2. This can be explained with the high amount of steam and the increased catalytic activity of the smaller olivine particles due to their increased specific surface. The lowest content of CO_2 and the highest CO content were reached in OP3, compared to OP2, where the same particle size (fine particles) was used. From OP2 to OP3 only the steam-to-carbon ratio (φ_{SC}) was reduced from 2.1 to 1.3 kg_{H20}/kg_C, so the changed value of φ_{SC} can be considered responsible for this. Koppatz et al. [15] studied the influence of the steam-to-fuel ratio (φ_{SF}) for steam gasification of wood pellets and found that CO and CO_2, in particular, are influenced significantly if φ_{SF} drops below a certain value. For wood pellets this was between 0.84 and 0.74 $kg_{H20}/kg_{fuel,daf}$. This reduction of φ_{SF} caused an increase of CO and a decrease of CO_2 in the product gas. Only a minor effect of φ_{SF} was found for H_2 (decrease by lowering φ_{SF}) and CH_4 was not influenced noticeably. This effect was also observed for the gasification of

Table 6
Fluidization velocities and their ratios to minimal required values.

Value	Unit	OP1	OP2	OP3
Minimum fluidization velocity for d_{sv}, U_{mf}	m/s	0.13	0.07	0.07
Terminal velocity for d_{sv}, U_t	m/s	5.25	3.36	3.36
Superficial velocity gasification reactor, U_g	m/s	0.35	0.43	0.40
Fluidization number gasif. reactor, U_g/U_{mf}	–	2.71	6.00	5.58
Transport number gasif. reactor, U_g/U_t	–	0.07	0.13	0.12
Superficial velocity comb. reactor, U_c	m/s	8.90	7.80	8.90
Fluidization number comb. reactor, U_c/U_{mf}	–	68.46	108.33	123.61
Transport number comb. reactor, U_c/U_t	–	1.70	2.32	2.65

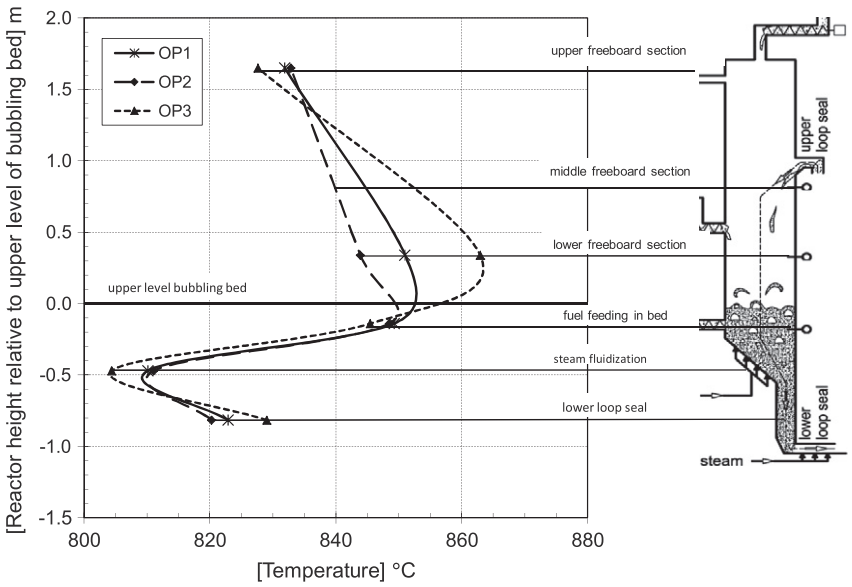

Fig. 6. Temperature profile in the gasification reactor.

lignite in the case here. The lower value of φ_{SC} for OP3 led to a drop of H_2 of 1.31 vol.%$_{db}$, an increase of CO of 4.17 vol.%$_{db}$ and CO_2 went down by about 2.14 vol.%$_{db}$. The amounts of H_2S and NH_3 were measured during the operation of OP1 and the results are summarized in Table 7. These impurities are formed by the sulfur and nitrogen content of the lignite. Previous research showed that nearly all of the introduced nitrogen is released in the gasification reactor [10,14]. Khan [30] found in his investigation that about 31% of the sulfur in the coal appears in the gaseous products ($H_2S + COS$) for coal pyrolysis whereas 19% of the H_2S content in the gas has to be added for COS compounds. CS_2 is generally a product of secondary reactions of COS and H_2S, but only to a negligible extent, as these reactions only occur at temperatures above 850 °C [31]. Due to this fact the estimated amount of COS in the gas can be up to 144 ppm$_v$, but due to the reducing atmosphere during steam gasification, this value can be taken as the maximum possible amount of COS. In a dual fluidized bed gasifier it has been found that the release of H_2S in the product gas is between 50 and 90% of the amount of sulfur introduced with the feedstock, while the difference leaves the system as SO_2 in the combustion reactor [10,14].

The detected product gas pollutants entrained dust and char are shown in Fig. 8. The dust content is made of the fuel ash and some attrition of the bed material. The attrition is affected only marginally by the changed conditions. For OP3 it can be guessed that the lower fluidization velocities, lower turbulence in the bed and, therefore, lower attrition rates of the olivine particles occur. Concerning the entrained char, the operation at OP2 caused the highest amount of entrained char in the gas compared to OP3 where the lowest values of char were detected. A reason for this could be the improved intermixing by higher gas velocities in the reactor at OP2. This could lead to a faster transport of the fuel to the bed surface, entrainment of char and forced abrasion of the char particles in the bed. By lowering φ_{SC}, (OP3) the amount of char found in the product gas was reduced by 58% compared to OP2 mainly because a lower fluidization velocity (steam) reduces the entrainment of fine particles.

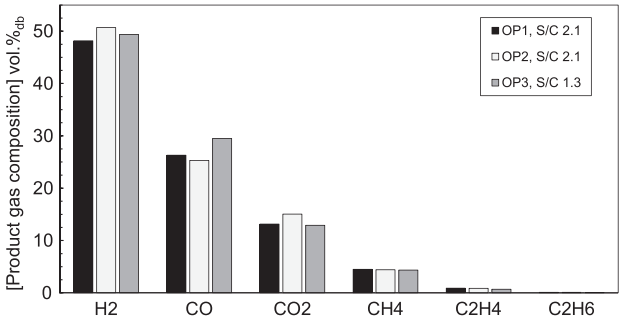

Fig. 7. Measured permanent gas composition in the product gas.

4.4. Tar content

For each operating point, various tar samples were taken and analyzed. The amounts of tar are shown in Fig. 9 (gravimetric tar and GC–MS tar). The amount of gravimetric- and GC–MS-detectable tar was in a narrow window between 3.0 and 3.3 g/Nm$^3_{db}$ of GC–MS-detectable tar and 0.7 and 1.0 g/Nm$^3_{db}$ of gravimetrically detectable tar. Koppatz et al. [32] found a massive decrease of the GC–MS tar in the case of smaller olivine particles, but in this study the particle size was even smaller with $d_{p50} = 260$ µm and the feedstock was biomass, which makes the result more distinctive than here. However, a reduction of the GC–MS tar cannot be observed here. This can be caused by the nature of the feedstock, as biomass causes, in general, more tar due to a higher content of devolatilization products in the gas. Nevertheless, a slight reduction of gravimetric tar can be observed.

By GC–MS analysis also individual tar components can be detected. A classification of these tar components can be made by using several factors. Milne et al. [33] categorized the components into primary, secondary and tertiary tar components depending on their temperature of formation. Another classification can be made when the individual components are dedicated to their super ordinated groups [34]. These groups are phenolic compounds, furans, aromatic compounds and polyaromatic hydrocarbons (PAH). Naphthalene, as the most dominant and most stable tar component, would belong to the group of PAH. To make the content of naphthalene visible, it will be removed from the group of PAH and treated separately. A third, widely used, classification is the characterization according to ECN [35]. Here, tars are classified into five tar classes. Class I contains tars that are non-detectable by

Table 7
Detected concentrations of ammonia and hydrogen sulfide in the product gas.

Value	Unit	OP1
NH_3	ppm$_v$	4710
H_2S	ppm$_v$	762

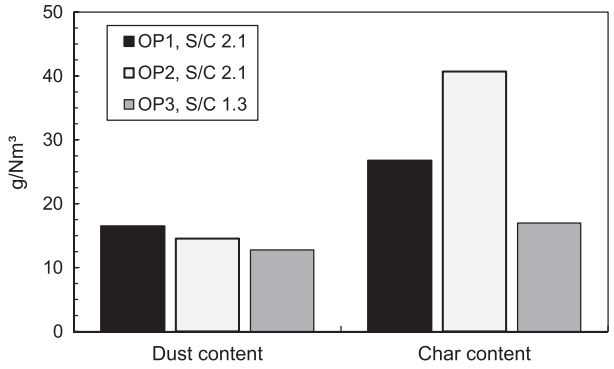

Fig. 8. Detected inorganic (dust) and organic (char) particulate matter in the product gas.

GC–MS as they condense at high temperatures (gravimetric tar). These tars have a high molecular weight. The other tar classes (II to V) are lighter hydrocarbons that are present in the tar. The complete classification of the individual GC–MS tar components according to the classifications discussed here is given in Table 8. The allocation of the GC–MS tar components to the ECN groups is provided in Fig. 10 and to the classification into primary, secondary and tertiary tars is given in Fig. 11. It can be seen that the tar classes are not influenced by the different operation points in an effective way. For detailed information about the GC–MS tar composition, Table 9 summarizes the amount and the relative contribution of the tar compounds. It can be seen that the different particle sizes do not influence significantly the amounts of the tar components. The reduced steam-to-carbon ratio of OP3 caused some slight changes, like a reduction of indene, phenol, styrene and benzofuran, and a small increase of fluoranthene.

Summing up the results of the tar measurements, a significant influence of the particle size of the bed material and the steam-to-carbon ratio could not be detected. Nevertheless, the tar production was already at a quite low level. In addition to the lower content of volatile components compared to biomass, there can also be a catalytic effect of the lignite ash responsible for these low tar yields. The effect of this mix of inorganic species in the system must not be neglected, as an ash mass flow of 0.58 kg/h was introduced by the lignite into the gasifier. The composition of the ash was detected by X-ray fluorescence (XRF) analysis. These results are listed in Table 10, which exposes the main components as calcium, sulfur, magnesium, iron and sodium. The high content of Fe_2O_3 is promising in this case due to the reason that a high content of Fe_2O_3 in combination with calcium works very well for tar-reducing catalytic reactions. Several research groups [36,37] identified iron(III) as the active part for catalytic reactions

Table 8
Classification of GC/MS tar components according to Milne [46] and ECN [48].

ECN Class	Component	Milne
Class II	Phenol	Primary/secondary
	2-methylphenol	Primary/secondary
	4-methylphenol	Primary/secondary
	Benzofuran	Secondary
	1H-indene	Secondary/tertiary
	Isoeugenol	Primary
	Isoquinoline	Secondary
	Quinoline	Secondary
Class III	Styrene	Secondary/tertiary
	Mesitylene	Tertiary
	Phenylacetylene	Tertiary
Class IV	Naphthalene	Secondary/tertiary
	2-methylnaphtalene	Secondary/tertiary
	1-methylnaphtalene	Secondary/tertiary
	Biphenyl	Secondary/tertiary
	Acenaphthylene	Tertiary
	Acenaphthene	Tertiary
	Anthracene	Tertiary
	Phenanthrene	Tertiary
	Dibenzofuran	Secondary
	Fluorene	Tertiary
	Fluoranthene	Tertiary
	4.5-methylphenanthrene	Secondary
	9-methylanthracene	Tertiary
Class V	Pyrene	Tertiary
	Benzo(b)fluoranthene	Tertiary
	Benzo(k)fluoranthene	Tertiary
	Benzo(ghi)perylene	Tertiary
	Benzo(a)pyrene	Tertiary
	Indenol[1,2,3]pyrene	Tertiary

regarding tar reduction. The latter researchers found that dolomite with a higher content of Fe_2O_3 performed better for tar conversion, which is an indicator for the catalytic activity. For steam reforming reactions, alkali metals are also catalytically active. It has been found that potassium carbonate is the most active species followed by sodium carbonate [38]. The potassium content of the ash can be neglected here compared to other fuels [39], but the sodium present in the ash is able to contribute significantly to the catalytic activity.

4.5. Product gas yield and conversion performance

The produced amount of product gas as well as the conversion of water and carbon into product gas will be discussed in this section. Essential characteristic values are summarized in Table 11. The product gas yield and the product gas-to-fuel ratio are shown in Fig. 12. The amount of product gas increased using fine bed material particles. The

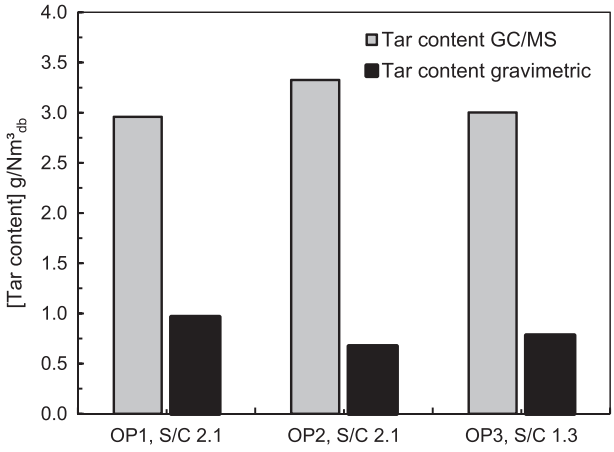

Fig. 9. GC–MS and gravimetric tar content in the product gas.

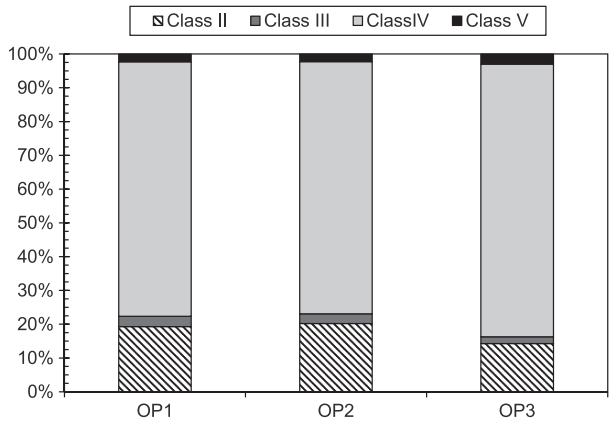

Fig. 10. GC–MS tar classification according to ECN [35].

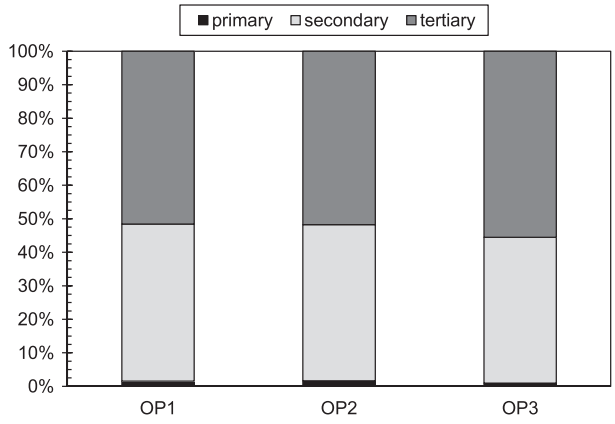

Fig. 11. GC–MS tar classification according to Milne [33].

dry product gas volume increased about 15.7% for OP2 compared to OP1. This effect can be caused by the increased contact with the hot bed material. The increased fluidization number at OP2 is a good indicator for this. At OP3 (lower steam-to-carbon ratio (φ_{SC})), the amount of product gas increased again about 5.8% compared to OP2. A similar trend was observed for the relative water conversion and the carbon conversion in the gasification reactor (Fig. 13). The carbon conversion in the gasifier increased from OP1 towards OP3. The relative water conversion goes along with these trends, but for OP3 this behavior is a special case: The water conversion increased from 0.52 at OP2 to 0.55 $kg_{H2O}/kg_{fuel,daf}$ at OP3 while the amount of steam that is provided for gasification was reduced with the lower steam-to carbon-ratio. As already guessed during discussion of the temperature profile of the reactor, the gasification reactions were enhanced at OP3, which goes along with the required fuel for the combustion reactor (Fig. 14). The overall reason for this effect can be ascribed to an increased residence time of the fuel and char particles in the gasification reactor by the changed fluidization regime in the following section:

The fluidization velocity for OP3 was lower, compared to OP2, as less steam was introduced into the bubbling bed at OP3, so also the fluidization number in the bubbling bed of the gasification reactor was lower (Table 6). It can be assumed that this reduction of steam fluidization had an influence on the movement of bed material and char to the combustion reactor. In other words, the bed material circulating rate between the reactors was reduced simultaneously. The net effect of this was that less char was transported to the combustion reactor while the char content in the gasification reactor was higher. The combination of the higher char content and the increased residence time in of the char and fuel particles in the gasification reactor caused a more intense contact of the steam with char and led to an increased amount of product gas and a better water conversion rate. As less char was

Table 9
Detected GC/MS tar components and their absolute and relative amount.

	OP1	OP2	OP3	OP1	OP2	OP3
Component	mg/Nm³			wt.%		
Naphthalene	1010.0	1093.4	1094.3	34.13	32.87	36.46
Indene	417.8	489.6	328.6	14.12	14.72	10.95
Acenaphthylene	300.8	379.3	381.8	10.16	11.40	12.72
Anthracene	181.7	205.4	217.2	6.14	6.18	7.24
2-Methylnaphthalene	107.1	115.0	60.7	3.62	3.46	2.02
Fluorene	113.5	140.8	121.6	3.84	4.23	4.05
Fluoranthene	85.0	100.9	127.5	2.87	3.03	4.25
Dibenzofuran	93.9	95.7	94.8	3.17	2.88	3.16
Phenanthrene	87.3	86.4	89.5	2.95	2.60	2.98
Pyrene	62.3	69.4	82.4	2.11	2.09	2.75
Phenol	66.1	77.8	40.2	2.23	2.34	1.34
Styrene	66.4	71.9	35.9	2.24	2.16	1.20
4,5-Methylphenanthrene	53.6	57.7	61.2	1.81	1.73	2.04
1-Methylnapthalene	55.2	52.9	40.7	1.86	1.59	1.36
Acenaphthene	43.2	43.2	33.2	1.46	1.30	1.11
Biphenyl	40.1	42.0	26.7	1.35	1.26	0.89
1-Benzothiophene	37.9	37.8	32.4	1.28	1.14	1.08
Quinoline	34.6	34.6	30.4	1.17	1.04	1.01
Benzofuran	27.3	29.5	10.0	0.92	0.89	0.33
Phenylacetylene	21.8	20.0	21.2	0.74	0.60	0.71
Chrysen	20.8	28.9	32.2	0.70	0.87	1.07
Benzo[a]anthracene	17.1	22.6	26.3	0.58	0.68	0.88
Rest	15.7	31.4	12.2	0.53	0.94	0.41
Sum	2959	3326	3001	100.00	100.00	100.00

Table 10
XRF analysis of the lignite ash.

Component	Unit	Amount
Na_2O	wt.%	4.51
MgO	wt.%	12.22
Al_2O_3	wt.%	1.58
SiO_2	wt.%	0.83
P_2O_5	wt.%	0.30
SO_3	wt.%	32.39
K_2O	wt.%	0.90
CaO	wt.%	36.11
TiO_2	wt.%	0.26
V_2O_5	wt.%	0.00
Cr_2O_3	wt.%	0.02
MnO	wt.%	0.13
Fe_2O_3	wt.%	10.01
NiO	wt.%	0.02
CuO	wt.%	0.02
ZnO	wt.%	0.01
Rb_2O	wt.%	0.00
SrO	wt.%	0.26
PbO	wt.%	0.00
Cl	wt.%	0.44

Table 11
Specific data of the accomplished tests.

Value	Unit	OP1	OP2	OP3
Total product gas amount	Nm^3/h	23.9	28.9	26.1
H_2O content in product gas	vol.%	25.8	28.7	19.1
Dry product gas amount	Nm^3_{db}/h	17.8	20.6	21.8
Specific product gas yield	$Nm^3_{db}/kg_{fuel,daf}$	1.32	1.54	1.65
Lower heating value	MJ/Nm^3_{db}	10.9	10.9	11.0
Chemical product gas power$_{excl.\ tar}$	kW	53.8	65.6	66.8
Cold gas efficiency, η_c	%	63.5	77.0	77.3
Specific H_2 yield	$Nm^3_{H2}/kg_{fuel,daf}$	0.644	0.762	0.820
Specific CO_2 yield	$Nm^3_{CO2}/kg_{fuel,daf}$	0.215	0.270	0.255
Specific CO yield	$Nm^3_{CO}/kg_{fuel,daf}$	0.380	0.415	0.486
Specific CH_4 yield	$Nm^3_{CH4}/kg_{fuel,daf}$	0.059	0.066	0.063
Specific C_2H_4 yield	$Nm^3_{C2H4}/kg_{fuel,daf}$	0.006	0.013	0.011
Specific C_2H_6 yield	$Nm^3_{C2H6}/kg_{fuel,daf}$	0.001	0.001	0.001
Logarithmic deviation from CO-shift equilibrium, $p\delta_{eq,CO\text{-}shift}$	–	−0.057	−0.061	0.164
Rel. water conversion, $X_{H20,rel}$	$kg_{H2O}/kg_{fuel,daf}$	0.418	0.522	0.549
Rel. water conversion, $X_{H20,rel}$	$kg_{H2O}/kg_{fuel,daf,N,S,Cl\ free}$	0.424	0.529	0.557
Stoichiometric steam demand	$kg_{H2O}/kg_{fuel,daf,N,S,Cl\ free}$		0.74	
Stoichiometric steam demand	$mol_{H2O}/kg_{fuel,daf,N,S,Cl\ free}$		41.06	
Ratio of water conversion to stoichiometric steam demand	kg_{H2O}/kg_{H2O}	0.57	0.71	0.75
Mean gas residence time in freeboard of gasification reactor, τ_F	S	4.7	3.8	4.1
Mean residence time in combustion reactor, τ_C	S	0.9	1.0	0.9

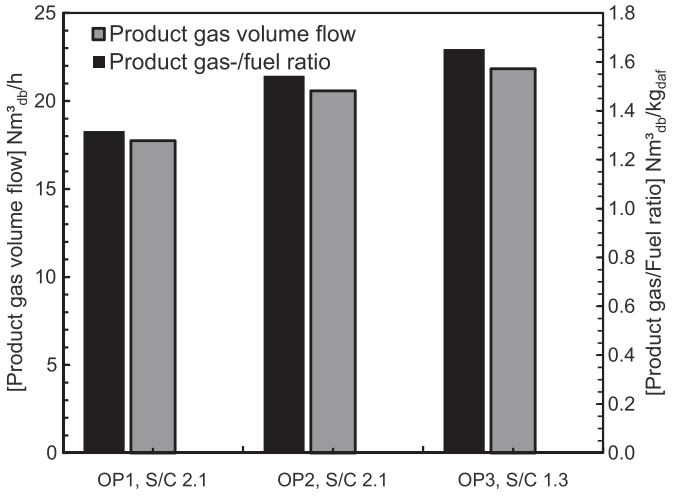

Fig. 12. Specific and absolute product gas amount.

transported to the combustion reactor while more char was gasified in the gasification reactor, more fuel for the combustion reactor was required to provide the heat for the gasification process (Fig. 14).

To provide a value for the efficiency of the gasification system, the cold gas efficiency is used here. For calculation of this value in case of tests on the pilot plant, it has to be kept in mind that a pilot plant usually does not reach the low ratio of heat losses like an industrial large-scale plant. In the case of the dual fluidized bed pilot plant, the heat losses are nearly 20% of the fuel input. A large scale plant can be operated with significantly lower heat losses. Stidl [40] calculated the heat losses by radiation for the main parts of the 10 MW_{th} dual fluidized bed gasification plant in Oberwart, Austria [6]. Based on the reported heat losses, the heat loss by radiation for an industrial plant can be assumed to be 2% of the input fuel power. To comparably use the cold gas efficiency for a plant of industrial size, Eq. (19) can be used.

$$\eta_C = \frac{\dot{V}_{PG} \cdot LHV_{PG}}{\left(P_{fuel,G} + P_{fuel,C} - \dot{Q}_{PP} + \dot{Q}_{IP}\right) \cdot 3600} \tag{19}$$

The gas composition itself is close to water–gas shift equilibrium (Table 11) for all operating points. For OP1 and OP2, $p\delta_{eq,CO\text{-}shift}$ was slightly below 0 whereas for OP3, $p\delta_{eq,CO\text{-}shift} > 0$. The small distance to equilibrium in all three cases was caused by the comparably high H_2

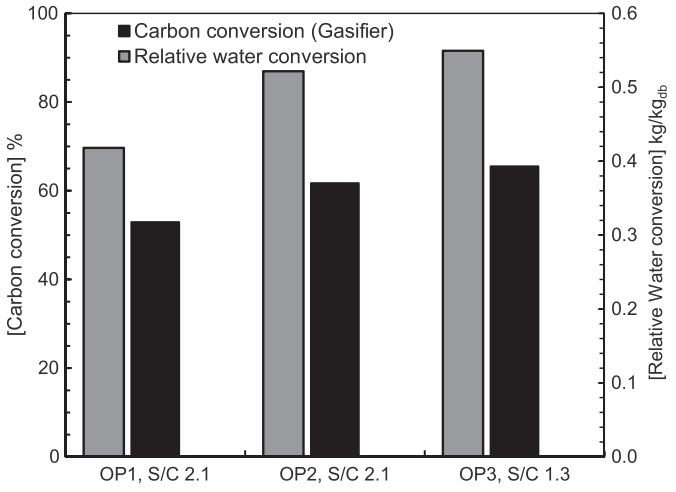

Fig. 13. Carbon conversion and water conversion in the gasification reactor.

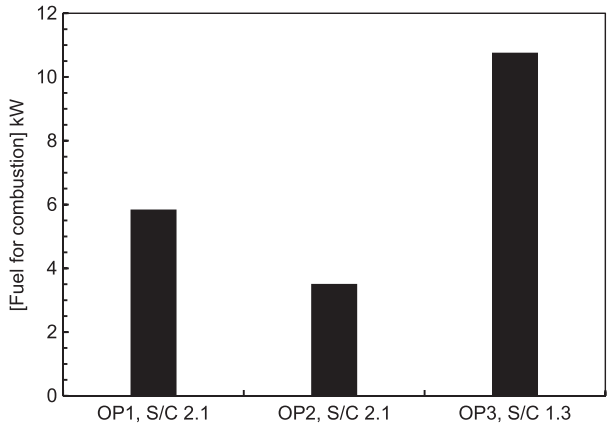

Fig. 14. Fuel for combustion (light heating oil).

content. In the case of OP3 the equilibrium is affected by the low water content in the gas and the high H_2 content. Here the reaction would try to shift the gas composition during passing the hot freeboard towards production of CO and H_2O, but due to the low residence time (τ_F) and the absence of a catalyst in the freeboard, this reaction was limited.

5. Conclusions

Steam gasification of lignite with two different sizes of bed materials and different ratios of steam in a dual fluidized bed (DFB) gasifier was successfully carried out with a fuel power of 90 kW at the DFB pilot plant at Vienna University of Technology. Variation of the bed material particle size and the amount of steam for gasification showed that the product gas quality was not affected for the used feedstock, but a noticeable influence on the performance for both measures (particle size and steam-to-carbon ratio) was found. The most significant changes by the smaller olivine particles (OP1 vs. OP2) used in this study are:

- Higher (+15.7%) product gas yield, higher cold gas efficiency.
- Increased carbon and water conversion in the gasification reactor by increased turbulence in the bubbling bed and enhanced contact to the bed material particles with larger surface.

The reduction of the bed material particle size offers the possibility to operate the gasification reactor with a lower amount of steam for fluidization, maintaining a good fluidization regime in the gasification reactor. The operation of the system with a lower amount of steam for gasification/fluidization showed an increase of performance data of the system, which can be detected by the following aspects (OP2 vs. OP3):

- Increased (+5.8%) product gas yield, higher cold gas efficiency.
- Higher carbon conversion was found in the gasification reactor. By the reduced rate of carbon from the gasification reactor to the combustion reactor, more char is held back in the bubbling bed of the gasification reactor and the steam-char contact was more intense. As a net effect of this (lower amount of char available for combustion), and the enhanced, energy consuming gasification reactions by the higher char content in the gasification reactor, the required additional fuel for the combustion reactor increased.
- Improved water conversion rate (goes along with the reasons explained for the higher carbon conversion).
- Lower water content of the product gas: By the combination of increased water conversion with a lower amount of steam present in the gasifier, a comparably low amount of unconverted water was left in the product gas.

Summarizing, the tests carried out showed that dual fluidized bed gasifier originally designed for the gasification of woody biomass can handle the lignite used as feedstock. Furthermore the performance and the efficiency of the gasification process for lignite as a feedstock

and olivine as the bed material can be improved by reduction of the bed material particle size and limitation of the amount of steam introduced into the gasification reactor.

Nomenclature

Symbols

d_P	General particle diameter μm
d_{P10}	Particle size with mass fraction <10% μm
d_{P50}	Mean particle size μm
d_{P90}	Particle size with mass fraction >90% μm
d_{sv}	Particle Sauter diameter μm
$d_{sv,f}$	Sauter diameter of the fine bed material used μm
$d_{sv,c}$	Sauter diameter of the coarse bed material used μm
$\Delta H_{R,850}$	heat of reaction at 850 °C kJ/mol
$K_{p,CO\text{-}shift}$	Equilibrium constant of CO-shift -
LHV_{PG}	Lower heating value of the product gas (dry) MJ/Nm^3_{db}
$\dot{m}_{H_2O,actual}$	Actual mass flux of steam in the gasification reactor kg/h
$\dot{m}_{H_2O,stoich.}$	Actual mass flux of steam in the gasification reactor kg/h
$\dot{m}_{steam}$	Mass flux of steam in the gasification reactor kg/h
$\dot{m}_{fuel}$	Mass flux of solid fuel into the gasification reactor kg/h
$\dot{m}_{H_2O,con.}$	Amount of water that is converted to product gas kg/h
$\dot{m}_{C_{PG}}$	Carbon flux in the product gas stream kg/h
P_i	actual measured gas phase partial pressure of the species *i* Pa
$p\delta_{eq,CO\text{-}shift}$	Logarithmic deviation from CO-shift equilibrium -
$P_{fuel,G}$	Input fuel power of solid fuel into gasification reactor kW
$P_{fuel,C}$	Input fuel power of fuel for combustion reactor kW
$\dot{Q}_{PP}$	Heat loss of the pilot plant kW
$\dot{Q}_{IP}$	Heat loss of an industrial size plant with the same fuel power as the pilot plant kW
U_{mf}	Minimum fluidization velocity for a single particle m/s
U_t	Terminal velocity for a single particle m/s
U_g, U_c	Superficial gas velocity in gasification reactor (g) and combustion reactor (c) m/s
$\dot{V}_{PG}$	Volumetric flow rate of product gas (dry) Nm^3_{db}/h
$X_{H_2O,rel}$	Water conversion in the gasifier, related to the fuel input $kg_{H2O}/kg_{fuel,daf}$
x	Molarity of carbon in the fuel (dry, ash, N, Cl and S free basis) $mol/kg_{C,H,O}$
y	Molarity of hydrogen in the fuel (dry, ash, N, Cl and S free basis) $mol/kg_{C,H,O}$
z	Molarity of oxygen in the fuel (dry, ash, N, Cl and S free basis) $mol/kg_{C,H,O}$

Greek letters

δ	Deviation -
ϕ_{H_2O}	Stoichiometric H_2O demand $mol_{H_2O}/kg_{daf,N,S,Cl\ free}$, $kg_{H_2O}/kg_{daf,N,S,Cl\ free}$
η_C	Cold gas efficiency -
$\varphi_{SF,wt}$	Steam-to-fuel ratio $kg_{H2O}/kg_{fuel,daf}$, -
$\varphi_{SC,wt}$	Steam-to-carbon ratio kg_{H2O}/kg_C, -
$\varphi_{SC,mol}$	Molar steam-to-carbon ratio mol_{H2O}/mol_C, -
λ_{H_2O}	Stoichiometric H_2O ratio mol/mol, kg/kg
τ_F	Product gas residence time in the freeboard of the gasification reactor s
τ_C	Gas residence time in the combustion reactor s
ν_{ash}	Ash mass fraction in the fuel -
ν_C	Carbon mass fraction in the fuel -
ν_{H_2O}	Water mass fraction in the fuel -

Abbreviations & subscripts

BTX	Benzene, toluene, xylene
c	Carbon, cold gas (efficiency), combustion reactor
CHP	Combined heat and power plant
daf	Dry and ash free basis
db	Dry basis
DFB	Dual fluidized bed
g	Gasification reactor
GC–MS	Gas chromatography mass spectrometry
IPA	Isopropanol
OP	Operating point
PAH	Polycyclic aromatic hydrocarbons
PG	Product gas
VUT	Vienna University of Technology
XRF	X-ray fluorescence

Acknowledgements

The authors gratefully acknowledge the financial support granted by the European Commission as this study was carried out within the framework of the Fecundus project, funded by the Research Fund for Coal and Steel of the European Union (Contract No RFCR-CT-2010-00009).

References

[1] A.V. Bridgwater, The technical and economic feasibility of biomass gasification for power generation, Fuel 74 (1995) 631–653.
[2] S. Rapagna, N. Jand, A. Kiennemann, P.U. Foscolo, Steam-gasification of biomass in a fluidized-bed of olivine particles, Biomass and Bioenergy 19 (2000) 187–197.
[3] G. Schuster, G. Löffler, K. Weigl, H. Hofbauer, Biomass steam gasification — an extensive parametric modeling study, Bioresource Technology 77 (2001) 71–79.
[4] K. Göransson, U. Söderlind, J. He, W. Zhang, Review of syngas production via biomass DFBGs, Renewable & Sustainable Energy Reviews 15 (2011) 482–492.
[5] H. Hofbauer, R. Rauch, K. Bosch, R. Koch, C. Aichernig, Biomass CHP plant Güssing — a success story, in: A.V. Bridgewater (Ed.), Pyrolysis and Gasification of Biomass and Waste, CPL Press, Newbury, Berks., UK, 2003, pp. 527–536.
[6] J. Kotik, Über den Einsatz von Kraft-Wärme-Kopplungsanlagen auf Basis der Wirbelschicht-Dampfvergasung fester Biomasse am Beispiel des Biomassekraftwerks Oberwart, PhD thesis, Vienna University of Technology, (written in German) 2010.
[7] T. Klotz, A regional energy-supply-showcase — the 15 MW fuel-power biomass gasification plant Villach, International Seminar on Gasification, Gothenburg, Sweden, 2010.
[8] I. Gunnarsson, The GoBiGas project — efficient transfer of biomass to biofuels, International Seminar on Gasification, Gothenburg, Sweden, 2010.
[9] C. Pfeifer, S. Koppatz, H. Hofbauer, Steam gasification of various feedstocks at a dual fluidised bed gasifier: impacts of operation conditions and bed materials, Biomass Conversion and Biorefinery 1 (2011) 39–53.
[10] S. Kern, C. Pfeifer, H. Hofbauer, Dual fluidized-bed steam gasification of solid feedstock: matching syngas requirements with fuel mixtures, in: T. Luckos, P. den Hoed (Eds.), Proceedings of Industrial Fluidization South Africa (IFSA 2011), Johannesburg, South Africa, 2011, pp. 67–78.
[11] J.C. Schmid, U. Wolfesberger, S. Koppatz, C. Pfeifer, H. Hofbauer, Variation of feedstock in a dual fluidized bed steam gasifier — influence on product gas, tar content and composition, Environmental Progress & Sustainable Energy 31 (2011) 205–215.
[12] V. Wilk, S. Kern, H. Kitzler, S. Koppatz, J.C. Schmid, H. Hofbauer, Gasification of plastic residues in a dual fluidized bed gasifier — characteristics and performance compared to biomass, Proceedings of the International Conference on Polygeneration Strategies (ICPS11), Vienna, Austria, 2011, pp. 55–65.
[13] S. Kern, C. Pfeifer, H. Hofbauer, Synergetic utilization of renewable and fossil fuels: dual fluidized bed steam co-gasification of coal and wood, APCBEE Procedia 1 (2012) 136–140.
[14] S. Kern, C. Pfeifer, H. Hofbauer, Co-gasification of wood and hard coal in a dual fluidized bed steam gasifier: process efficiency vs. gasification temperature, Proceedings of the 21st International Conference on Fluidized Bed Combustion (FBC), Naples, Italy, June 2012, pp. 744–751.
[15] S. Koppatz, C. Pfeifer, H. Hofbauer, Comparison of the performance behaviour of silica sand and olivine in a dual fluidised bed reactor system for steam gasification of biomass at pilot plant scale, Chemical Engineering Journal 175 (2011) 468–483.
[16] C. Pfeifer, S. Koppatz, H. Hofbauer, Catalysts for dual fluidised bed biomass gasification-an experimental study at the pilot plant scale, Biomass Conversion and Biorefinery 1 (2011) 1–12.
[17] A.G. Collot, Matching gasification technologies to coal properties, International Journal of Coal Geology 65 (2006) 191–212.
[18] K. Miura, K. Hashimoto, P.L. Silveston, Factors affecting the reactivity of coal chars during gasification, and indices representing reactivity, Fuel 68 (1989) 1461–1475.
[19] R.K. Boyd, P.J. Benyon, Coal property impacts on gasification, Proceedings of: Research symposium on entrained-flow gasification, CRC Black Coal Utilisation, Advanced technology Centre, Callaghan, NSW, Australia, 1999.
[20] M. Kaltschmitt, H. Hartmann, H. Hofbauer, Energie aus Biomasse, Springer, Berlin, Heidelberg, 2009.
[21] HSC, HSC Chemistry 5.1, Outokumpu Research Oy, Pori, Finland, 2002.
[22] F. Kirnbauer, V. Wilk, H. Kitzler, S. Kern, H. Hofbauer, The positive effects of bed material coating on tar reduction in a dual fluidized bed gasifier, Fuel 95 (2012) 553–562.

[23] S. Kern, C. Pfeifer, H. Hofbauer, Gasification of wood in a dual fluidized bed gasifier: influence of fuel feeding on process performance, Chemical Engineering Science 90 (2013) 284–298.
[24] J.P.A. Neft, H.A.M. Knoef, U. Zielke, K. Sjöström, P. Hasler, P.A. Simell, M.A. Dorrington, L. Thomas, N. Abatzoglou, S. Deutch, C. Greil, G.J. Buffinga, C. Brage, M. Suomalainen, Guideline for Sampling and Analysis of Tar and Particles in Biomass Producer Gases, ERK6-CT1999-20002, Version 3.3, ECN , 1999.
[25] E. Perz, A computer method for thermal power cycle calculation, Journal of Engineering for Gas Turbines and Power 113 (2) (1991) 184–189.
[26] L. Devi, M. Craje, P. Thüne, K.J. Ptasinski, F.J.J.G. Janssen, Olivine as tar removal catalyst for biomass gasifiers: Catalyst characterization, Applied Catalysis A: General 294 (2005) 68–79.
[27] R. Rauch, C. Pfeifer, K. Bosch, H. Hofbauer, D. Świerczyński, C. Courson, et al., Comparison of different olivines for biomass steam gasification, Proceedings of the Conference for Science in Thermal and Chemical Biomass Conversion, Victoria, Canada, vol. 1, 2004, pp. 799–809.
[28] F. Kirnbauer, H. Hofbauer, Investigations on bed material changes in a dual fluidized bed steam gasification plant in Güssing, Austria, Energy & Fuels 25 (2011) 3793–3798.
[29] D. Geldart, Types of gas fluidization, Powder Technology 7 (1973) 285–292.
[30] M.R. Khan, Prediction of sulphur distribution in products during low temperature coal pyrolysis and gasification, Fuel 68 (1989) 1439–1449.
[31] W.H. Calkins, Investigation of organic sulfur-containing structures in coal by flash pyrolysis experiments, Energy & Fuels 1 (1987) 59–64.
[32] S. Koppatz, J.C. Schmid, C. Pfeifer, H. Hofbauer, The Effect of Bed Particle Inventories with Different Particle Sizes in a Dual Fluidized Bed Pilot Plant for Biomass Steam Gasification, Industrial and Engineering Chemistry Research (2012), http://dx.doi.org/10.1021/ie202353b.
[33] T.A. Milne, N. Abatzoglou, R.J. Evans, Biomass Gasifier 'Tars': Their Nature, Formation, and Conversion, National Renewable Energy Lab, Golden, CO, USA, 1998.
[34] U. Wolfesberger, S. Koppatz, C. Pfeifer, H. Hofbauer, Effect of iron supported olivine on the distribution of tar compounds derived by steam gasification of biomass, Proceedings of the International Conference on Polygeneration Strategies (ICPS11), Vienna, Austria, 2011, pp. 69–76.
[35] ECN, Tar Classification System, http://www.thersites.nl2009.
[36] D. Świerczyński, C. Courson, L. Bedel, A. Kiennemann, J. Guille, Characterization of Ni – Fe/MgO/Olivine Catalyst for Fluidized Bed Steam Gasification of Biomass, Chemistry of Materials 18 (17) (2006) 4025–4032.
[37] A. Orio, J. Corella, I. Narváez, Performance of Different Dolomites on Hot Raw Gas Cleaning from Biomass Gasification with Air, Industrial and Engineering Chemistry Research 36 (1997) 3800–3808.
[38] L.K. Mudge, E.G. Baker, D.H. Mitchell, M.D. Brown, Catalytic steam gasification of biomass for methanol and methane production, Journal of Solar Energy Engineering 107 (1985) 88–92.
[39] H. Kitzler, C. Pfeifer, H. Hofbauer, Gasification of different kinds of non woody biomass in a 100 kW dual fluidized bed gasifier, Proceedings of the 21st International Conference on Fluidized Bed Combustion (FBC), Naples, Italy, June 2012, pp. 760–766.
[40] M. Stidl, Prozesssimulation von spezifischen Anwendungsfällen der Zweibett-Wirbelschicht-Dampfvergasungs-Technologie für die Papier- und Zellstoffindustrie, PhD Thesis, Vienna University of Technology, 2012, pp. 112.